Development/Plasticity/Repair

Strong Gamma Frequency Oscillations in the Adolescent Prefrontal Cortex

Zhengyang Wang,[1] Balbir Singh,[2] Xin Zhou,[2,3,4] and Christos Constantinidis[1,2,5]

[1]Neuroscience Program, Vanderbilt University, Nashville, Tennessee 37235, [2]Department of Biomedical Engineering, Vanderbilt University, Nashville, Tennessee 37235, [3]Department of Computer Science, Vanderbilt University, Nashville, Tennessee 37235, [4]Data Science Institute, Vanderbilt University, Nashville, Tennessee 37235, and [5]Department of Ophthalmology and Visual Sciences, Vanderbilt University Medical Center, Nashville, Tennessee 37232

Working memory ability continues to mature into adulthood in humans and nonhuman primates. At the single-neuron level, adolescent development is characterized by increased prefrontal firing rate in the delay period, but less is known about how coordinated activity between neurons is altered. Local field potentials (LFPs) provide a window into the computations conducted by the local network. To address the effects of adolescent development on LFP activity, three male rhesus monkeys were trained to perform an oculomotor delayed response task and tested at both the adolescent and adult stages. Simultaneous single-unit and LFP signals were recorded from areas 8a and 46 of the dorsolateral prefrontal cortex. In both the cue and delay period, power relative to baseline in the gamma frequency range (32–128 Hz) was higher in the adolescent than the adult stage. The changes between developmental stages could not be accounted for by differences in performance and were observed in more posterior as well as more anterior recording sites. In the adult stage, high-firing neurons were also more likely to reside at sites with strong gamma power increase from baseline. For both stages, the gamma power increase in the delay was selective for sites with neuron-encoding stimulus information in their spiking. Our results establish gamma power decrease to be a feature of prefrontal cortical maturation.

Key words: **adolescence; local field potential; monkey; neurophysiology; prefrontal cortex**

Significance Statement

Gamma-frequency oscillations in extracellular field recordings (e.g., local field potential or EEG) are a marker of normal interactions between excitatory and inhibitory neurons in neural circuits. Abnormally low gamma power during working memory is seen in conditions such as schizophrenia. We sought to examine whether the immature prefrontal cortex similarly exhibits lower power in the gamma-frequency range during working memory, in a nonhuman primate model of adolescence. Contrary to this expectation, the adolescent PFC exhibited stronger gamma power during the maintenance of working memory. Our findings reveal an unknown developmental maturation trajectory of gamma-band oscillations, propose a refinement of information encoding during PFC maturation, and raise the possibility that schizophrenia represents an excessive state of prefrontal maturation.

Introduction

Human executive functions including working memory continue to mature after the onset of puberty (Fry and Hale, 2000; Gathercole et al., 2004; Davidson et al., 2006; Ullman et al., 2014). This pattern of maturation parallels continued structural changes in the prefrontal cortex: early childhood excitatory synaptogenesis is followed by synaptic pruning in adolescence (Bourgeois et al., 1994; Anderson et al., 1995; Huttenlocher and Dabholkar, 1997), along with decreasing cortical thickness and gray matter volume (Giedd and Rapoport, 2010). In tasks requiring working memory, human imaging studies have also reported distinct changes in prefrontal activity patterns in humans between childhood and adulthood (Luna et al., 2001; Bunge et al., 2002; Klingberg et al., 2002; Kwon et al., 2002; Olesen et al.,

Received Aug. 5, 2021; revised Dec. 31, 2021; accepted Feb. 16, 2022.

Author contributions: Z.W., X.Z., and C.C. designed research; B.S., X.Z., and C.C. performed research; B.S. and C.C. contributed unpublished reagents/analytic tools; Z.W., B.S., and X.Z. analyzed data; Z.W., B.S., X.Z., and C.C. wrote the paper.

The research reported in this study was supported by the National Institute of Mental Health of the National Institutes of Health under Grants R01 MH 117996 and R01 MH 116675. We thank Austin Lodish and Junda Zhu for technical and analytical help; and André Bastos, Beatriz Luna, and David Blake for helpful comments on the manuscript.

The authors declare no competing financial interests.

Correspondence should be addressed to Christos Constantinidis at Christos.constantinidis.1@vanderbilt.edu or Xin Zhou at Maizie.zhou@vanderbilt.edu.

https://doi.org/10.1523/JNEUROSCI.1604-21.2022

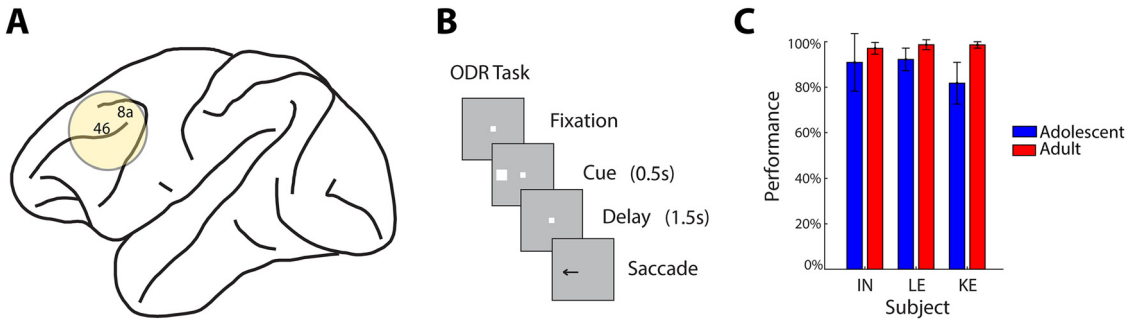

Figure 1. Brain regions recorded, task design, and behavior performance. ***A***, Schematic diagram of the monkey brain, with the locations of neurophysiological recordings in the dorsolateral prefrontal cortex indicated (areas 8a and 46). ***B***, The oculomotor delayed response task required the subject to saccade to a remembered location after a 1.5 s delay. ***C***, Behavior performance of the three subjects used in this study in two stages 1.6–2.1 years apart, referred to as the adolescent and adult stages. Mean percentage of correct trials in ODR task, excluding breaks in fixation, for: young, 88%; adult, 98%. Error bars represent the SD.

2003; Burgund et al., 2006; Olesen et al., 2007). Other markers of neuronal activity, including the distribution of power across different frequency bands of the EEG also changes markedly between the time of adolescence and adulthood (Uhlhaas et al., 2009). Gamma-band oscillations are thought to be driven primarily by excitatory–inhibitory neuronal loops (Buzsáki and Wang, 2012), thus suggesting that the strength of gamma oscillations can serve as a marker of synaptic maturation (Uhlhaas et al., 2010). Schizophrenia, a neurodevelopmental disorder with a typical early adulthood onset, is characterized by impaired working memory performance (Goldman-Rakic, 1994), abnormal trajectory of prefrontal interneuron maturation (Dienel and Lewis, 2019), as well as decreased power of gamma oscillations (Woo et al., 2010; Uhlhaas and Singer, 2013).

Nonhuman primates exhibit a strikingly similar pattern of cognitive development and prefrontal maturation (Constantinidis and Luna, 2019), and allow for more direct insights into the nature of neural changes that mediate these phenomena. Single-neuron recordings obtained in nonhuman primates at different developmental stages have thus revealed an increased firing rate specifically during the intervals of memory maintenance (Zhou et al., 2013, 2014, 2016b). Continued maturation of inhibitory connections has also been directly documented in the adolescent prefrontal cortex (Gonzalez-Burgos et al., 2015), as have changes in the effective, intrinsic connectivity among prefrontal neurons between adolescence and adulthood (Zhou et al., 2014). Analysis of neuronal rhythmicity in the adolescent primate prefrontal cortex has not been reported until now. Local field potentials (LFPs), a signal representative of the summation of postsynaptic activity in a small cortical volume (Kajikawa and Schroeder, 2011), provide a mesoscopic measure to link these empirical results. As in human EEG studies, working memory maintenance is generally characterized by elevated gamma-frequency power in the local field potential (Pesaran et al., 2002; Howard et al., 2003; Jensen et al., 2007; Honkanen et al., 2015; Kornblith et al., 2016).

We were thus motivated to determine whether prefrontal cortical maturation between adolescence and adulthood is characterized by increased gamma-band rhythmicity in the local field potential. We analyzed LFP recordings obtained from the same subjects as they transitioned from adolescence to adulthood (Zhou et al., 2016b,c). Unexpectedly, we found robust gamma-band oscillations in the adolescent prefrontal cortex that declined rather than increased during adulthood.

Materials and Methods

Subjects and data collection. Neurophysiological data used for analysis were collected from male rhesus monkeys performing a visual working memory task and reported in detail previously (Zhou et al., 2014, 2016a,c). All surgical and animal use procedures were reviewed and approved by the Wake Forest University Institutional Animal Care and Use Committee, in accordance with the US Public Health Service Policy on humane care and use of laboratory animals and the National Research Council *Guide for the Care and Use of Laboratory Animals*. Quarterly morphometric and hormonal measures were obtained to determine the onset of puberty as well as maturity of each animal.

The monkeys were trained to perform the oculomotor delayed response (ODR) task (Fig. 1). This task required the subject to remember the location of a 1° white square stimulus presented for 0.5 s following a 1 s fixation period. The stimulus could appear at one of eight locations arranged on a circle of 10° eccentricity. After a 1.5 s delay period, the fixation point was extinguished, prompting the subject to saccade to the remembered location within a 0.6 s time window to receive a liquid reward. The saccade end point had to deviate no more than 5–6° from the center of the stimulus. Correct trials were included for subsequent analysis.

Neural recordings were collected from areas 8a and 46 of the dorsolateral prefrontal cortex (dlPFC). Epoxylite-coated tungsten electrodes with a diameter of 250 μm and an impedance of 4 MΩ at 1 kHz (FHC) were acutely advanced into the brain, and a reference electrode was attached to the metal recording chamber. Spike waveforms were amplified, bandpass filtered between 0.5 and 8 kHz, and sampled at 40 kHz, while unipolar LFP traces were sampled continuously at 500 Hz. Both signals were digitized and stored through a modular data acquisition system (APM System, FHC).

The subjects were initially trained in adolescence until they reached asymptotic performance. Neurophysiological recordings were then collected for a period of ~6 months. Once these experiments were completed, the monkeys were no longer tested or trained in any task but remained in the colony for ~1.5 years, until they reached maturation. The subjects were then briefly reintroduced to the task, and a second phase of recording was then performed (Zhou et al., 2014, 2016a,c).

LFP signal processing. LFP recordings were processed using the FieldTrip (https://www.fieldtriptoolbox.org/) and Chronux (http://chronux.org/) toolboxes as well as custom MATLAB code in MATLAB 2018b (MathWorks). LFP signals of individual trials first underwent artifact rejection. Single-trial LFP traces were zero meaned and then bandpass filtered between 1 and 200 Hz with a zero-phase fifth-order Butterworth filter (10th order in effect) and then notch filtered at 60 Hz with a bandwidth of 0.2 Hz using the *ft_preproc_dftfilter* function. The signals were then standardized by their SD as estimated by the median absolute deviation. The spectrogram of single traces between 2 and 128 Hz were computed by the *mtspecgramc* function with six tapers of 500 ms time windows. LFP power in the alpha, beta, gamma, and high-gamma bands were defined to be the sum of power in the spectrogram between the frequencies of 8–16, 16–32, 32–64, and 64–128 Hz, respectively. We used the last 500 ms of the fixation period as the baseline period. Relative band power was calculated by dividing the sum of power

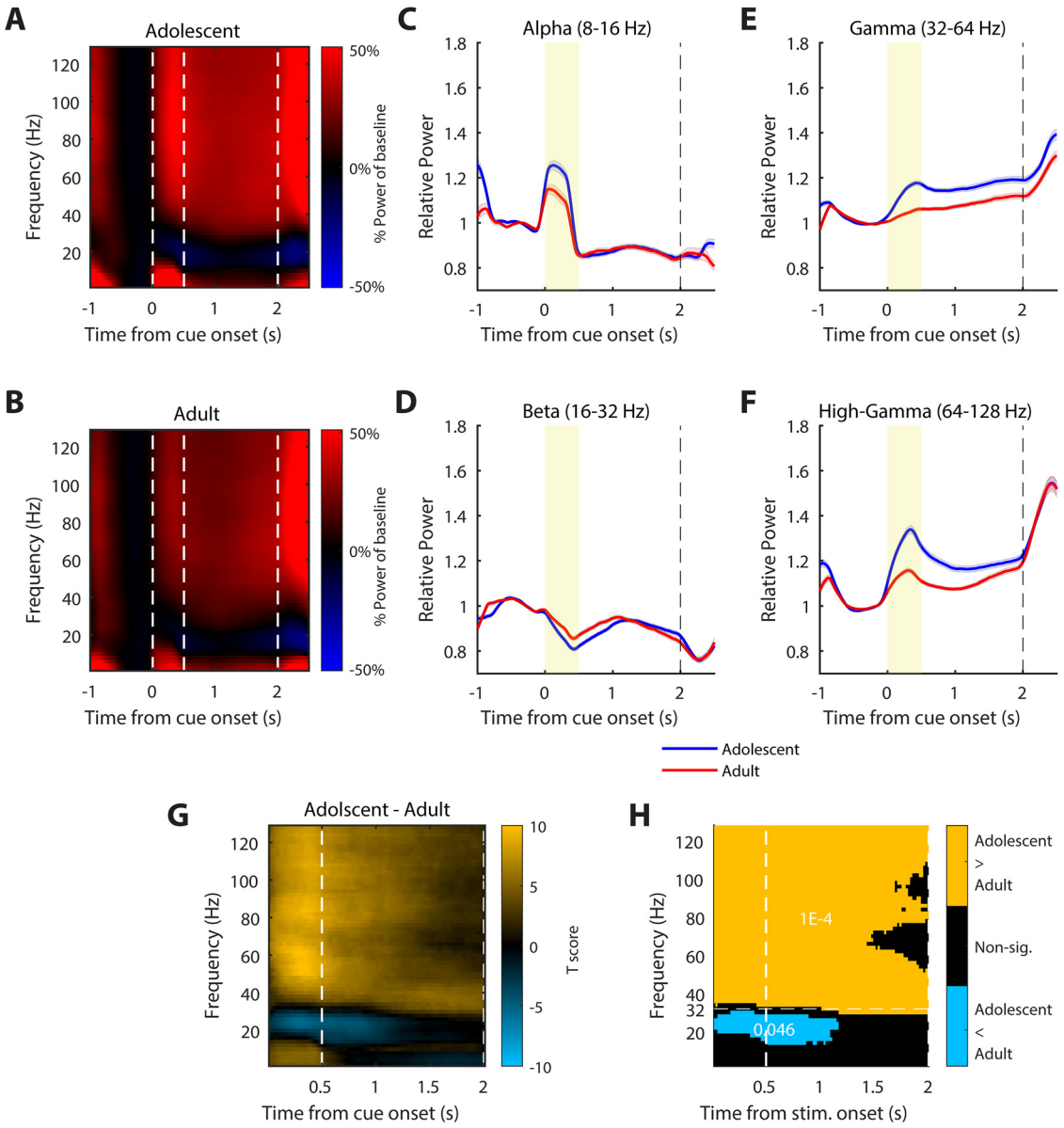

Figure 2. LFP power changes in dlPFC during adolescent development. ***A***, ***B***, Population average across electrodes and sessions of moment-by-moment LFP spectral power in proportion to that in the last 500 ms before cue onset for LFP recording sites at the adolescent ($N = 130$) and adult ($N = 164$) stages. ***C–F***, Population averages of LFP power evolutions aligned to cue onset in the frequency bands among 8–16, 16–32, 32–64, and 64–128 Hz at sites recorded in the adolescent ($N = 130$) and adult ($N = 164$) stages. Shaded areas represent the SEM. ***G***, Uncorrected two-sample t test values comparing the moment-by-moment LFP spectral power in proportion to that in the last 500 ms before cue onset between the adolescent ($N = 130$) and adult ($N = 164$) stages. Positive values correspond to larger adolescent power. ***H***, Significant clusters found in the permutation test based on t values in ***G***. The number in each cluster represents the bootstrapped p value.

within each band at each time point by the average of the sum in the baseline period. The values in the relative spectrograms (Fig. 2) were calculated separately at each frequency (at a 2 Hz resolution). To identify recording sites where LFP power was modulated in a specific frequency band, a two-tailed paired-sample t test was conducted on the band power from all trials at each recording site during the delay period vs. the baseline period. Sites with p values <0.05 were defined to be modulated in the corresponding frequency band. For each recording site, the preferred cue location of a certain LFP band was defined as the one that resulted in the largest LFP power in that frequency band during the delay period. To find spatially selective LFP recording sites, one-way ANOVA test was conducted on the band power of each recording site averaged during the delay period in response to different stimulus location. LFP recording sites with p values <0.05 were defined to be selective for stimulus location in the corresponding power band.

Spike processing. Recorded spike waveforms were sorted into separate units using a semi-automated cluster analysis method based on the KlustaKwik algorithm. A trial-averaged peristimulus time histogram (PSTH) was computed by convolving the spiking events with a 50 ms boxcar kernel at 20 ms steps apart. The evoked PSTH was calculated by subtracting the average firing rate in the 1 s fixation period. For each recorded neuron, its preferred cue location was defined as the one that resulted in the highest evoked firing rate during the delay period. Single-trial PSTH for computing moment-by-moment percentage of explained variance (PEV) used a 250 ms box kernel instead. Neurons were identified to be responsive to the task, if their activity increased significantly during any task epoch relative to the baseline fixation period, evaluated at the 0.05 significance level, as we have described previously (Zhou et al., 2016c). To identify neurons selective for spatial location during the delay period of the task, a one-way ANOVA was conducted on the firing rates of each neuron averaged during the entire delay period. Selective

neurons were defined to be the ones with p values <0.05. The bias-corrected PEV ω^2 was computed in Equation 1 at steps of 20 ms on the single-trial firing rate of each neuron, where MSE is the mean squared error within stimulus locations, df is the degree of freedom, $SS_{Between}$ is the sum of squares between stimulus locations, and SS_{total} is the total variance, as follows:

$$\omega^2 = \frac{ss_{Between} - df \times MSE}{ss_{Total} + MSE}. \quad (1)$$

Cluster-based permutation test. A permutation test with 10,000 iterations was conducted to compare the relative spectrogram between the adolescent and the adult using the FieldTrip function *ft_freqstatistics*. Two-tailed independent-sample t tests were first run for each time–frequency combination to generate uncorrected p values before connected regions of all positive or negative t statistics with p values <0.05 were identified (clusters). The sum of all t statistics within each cluster was calculated. The labels for developmental stage were then randomly shuffled 10,000 times where each time the largest cluster sum of t values was recorded. The original cluster sum of t values was then compared against the bootstrapped shuffled distribution to generate a one-tailed p value.

Correlation analysis. The neuron-by-neuron Spearman's correlation between neuronal firing rate/PEV and LFP power was computed by first averaging the signals within each neuron or recording site and within the delay period, and then matching the signals that were recorded from the same electrode in each session. The correlation coefficients were compared across the adolescent and the adult stage using Fisher's Z transform.

Temporal correlation was calculated for the time-series signals in the delay period of each trial. The spiking events were convolved with a 50 ms boxcar kernel. For each neuron, the trials for each stimulus location were concatenated, and the correlation was computed between the convolved spiking and the LFP power changes from baseline at each frequency. Only results from the stimulus location that resulted in the strongest evoked delay period firing rate for each neuron were further considered. When examined on a frequency-by-frequency basis, all p values were corrected for using the Bonferroni–Holm procedure (see the Statistics section that follows).

Statistics. All statistical tests were conducted using MATLAB 2018b. An α level of 0.05 was adopted for all tests. The familywise error rate was controlled for using the Bonferroni correction when multiple comparisons were conducted in multiple canonical frequency bands. For n comparisons, the Bonferroni correction sets the critical p value to α/n. Alternatively, the Bonferroni–Holm procedure was conducted when multiple comparisons were conducted in a frequency-by-frequency fashion. Briefly, the Bonferroni–Holm procedure sorts all p values from lowest to highest, then compares them in order from the first to the kth p value to a critical level of $\alpha/(n+1-k)$. A comparison is considered significant if the current p value is smaller than the critical level; otherwise, the current and all following comparisons are deemed not significant, and the procedure stops.

Results

LFP activity was recorded from dorsolateral prefrontal areas 8a and 46 (Fig. 1*A*) of three male Rhesus monkeys (*Macaca mulatta*), trained to perform the ODR task (Fig. 1*B*). The task tested the visual working memory ability of the animals by requiring the subject, after a delay of 1.5 s, to make a saccade to a remembered stimulus location that was presented for 0.5 s. The animals were tested at two stages of development: the "adolescent" stage after puberty onset (age, ~4.5 years) and the "adult" stage once development had completed (age, ~6.5 years). Young monkeys generally achieved a lower performance in the task than adult ones (Fig. 1*C*; 88% vs 98% correct performance for young and adult, respectively, not considering aborted trials), as we have reported previously (Zhou et al., 2016c). We analyzed LFP activity from electrodes where single-unit activity was also identified. The resulting dataset consisted of signals from 298 neurons and 130 LFP sites in the adolescent stage along with 392 neurons and 164 LFP sites in the adult stage.

Adolescent dlPFC shows a stronger pattern of LFP power modulation in the ODR task

We calculated LFP spectral power at each epoch of the ODR task, relative to baseline. For each recording session from one electrode, the baseline period for LFP analysis was defined to be the last 500 ms of the fixation period to avoid including the transient power changes following fixation onset. The relative power of the recording was then calculated as the spectrogram change from the baseline average at each respective frequency. Results from different sessions and electrodes were averaged together for the adolescent stage (Fig. 2*A*) and the adult stage (Fig. 2*B*), respectively. To describe in detail its temporal evolution throughout the different epochs of the task, LFP power modulation was evaluated in the following four different frequency bands: alpha (8–16 Hz), beta (16–32 Hz), gamma (32–64 Hz), and high gamma (64–128 Hz). The resulting relative power spectrogram showed similar patterns of modulations in each task epoch at the adolescent and adult stages (Fig. 2*C–F*). Specifically, gamma (Fig. 2*E*) and high-gamma (Fig. 2*F*) power were elevated relative to baseline during both the cue presentation and the delay period. Beta power (Fig. 2*D*) generally showed modulations in the opposite direction as gamma, showing decreases in both the cue and delay periods. Alpha-band power (Fig. 2*C*) had an initial increase during cue presentation and then quickly dropped below baseline in the delay period.

Contrary to our initial hypothesis, gamma-band and high gamma-band LFP power was more strongly elevated during the delay interval of the task in the adolescent than the adult stage (Fig. 2*E*,*F*). Averaged across the entire duration of the delay period, the difference was highly significant for the gamma range (two-tailed t test: $t_{(292)} = 5.09$, $p = 6.4E\text{-}7$) and high-gamma range (two-tailed t test $t_{(292)} = 4.86$, $p = 1.9E\text{-}6$). This difference was specific for the gamma and high-gamma frequency ranges. No significant difference was detected for the alpha or beta power (two-tailed t test: $t_{(292)} = -0.13$ and -0.68, respectively; $p = 0.89$ and 0.50, respectively). In addition, adult dlPFC neurons exhibited higher firing rates, both in terms of absolute firing rate and as an increase over the baseline (Zhou et al., 2016c). As a result, the difference in gamma and high-gamma power between the two stages cannot be accounted for by systematic differences in firing rate and in fact moved in the opposite direction than would be expected based on firing rate alone (further examined below).

Differences between stages in spectral power changes during the cue presentation and memory delay were further confirmed using a cluster-based permutation test (Fig. 2*G*,*H*) at every 2 Hz between 2 and 128 Hz. Consistent with findings in bandpass power, one strong cluster was identified: LFP power modulation above ~30 Hz was significantly higher ($p = 1.0E\text{-}4$) for the adolescent than the adult throughout the cue presentation and memory delay epochs. One other marginally significant ($p = 0.0457$) cluster was found, suggesting stronger negative modulation for the adolescent <30 Hz in an epoch immediately following cue presentation.

These changes in LFP power were consistent in subject KE and LE from whom there was a substantial amount of data (Fig. 3). Similar decreases in gamma power were also observed in both area 8a and area 46 (Fig. 4*A*,*B*). To also rule out potential biased

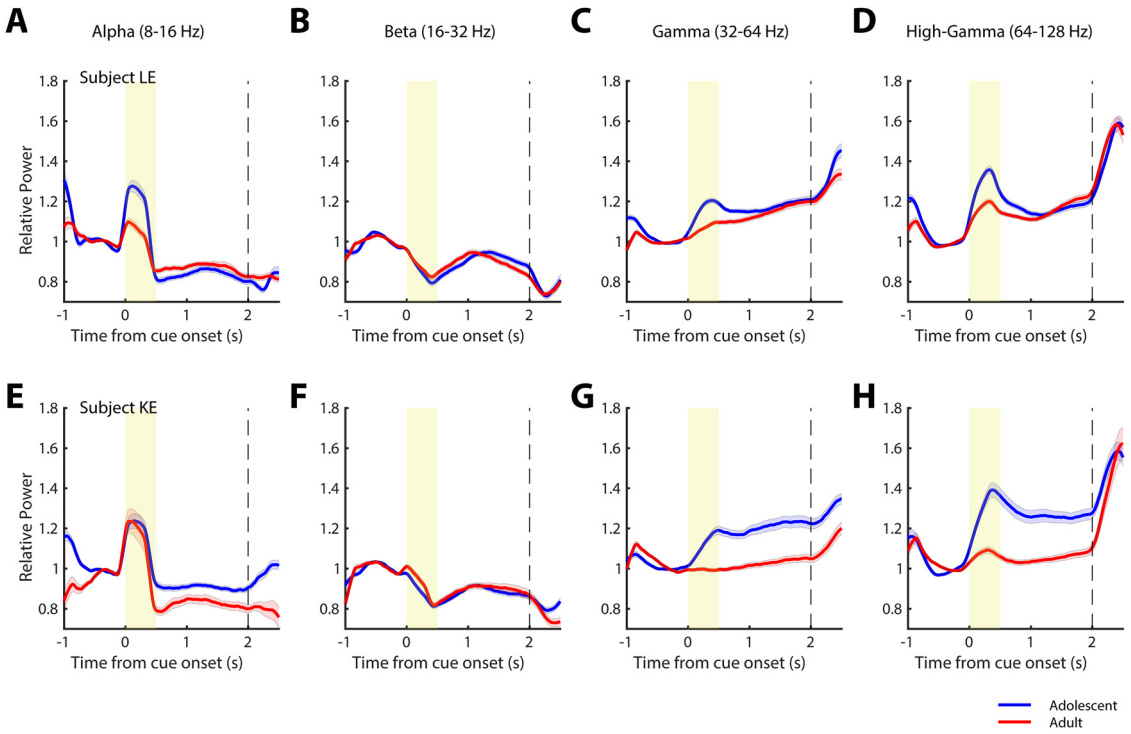

Figure 3. LFP power of different individual subjects. ***A–D***, Temporal evolution of alpha, beta, gamma, and high-gamma power aligned to cue onset for subject LE ($N = 77$ adolescent sites; $N = 90$ adult sites). ***E–H***, same as ***A–D*** but for subject KE ($N = 41$ adolescent sites; $N = 50$ adult sites). Conventions are the same as in Figure 2*C–F*.

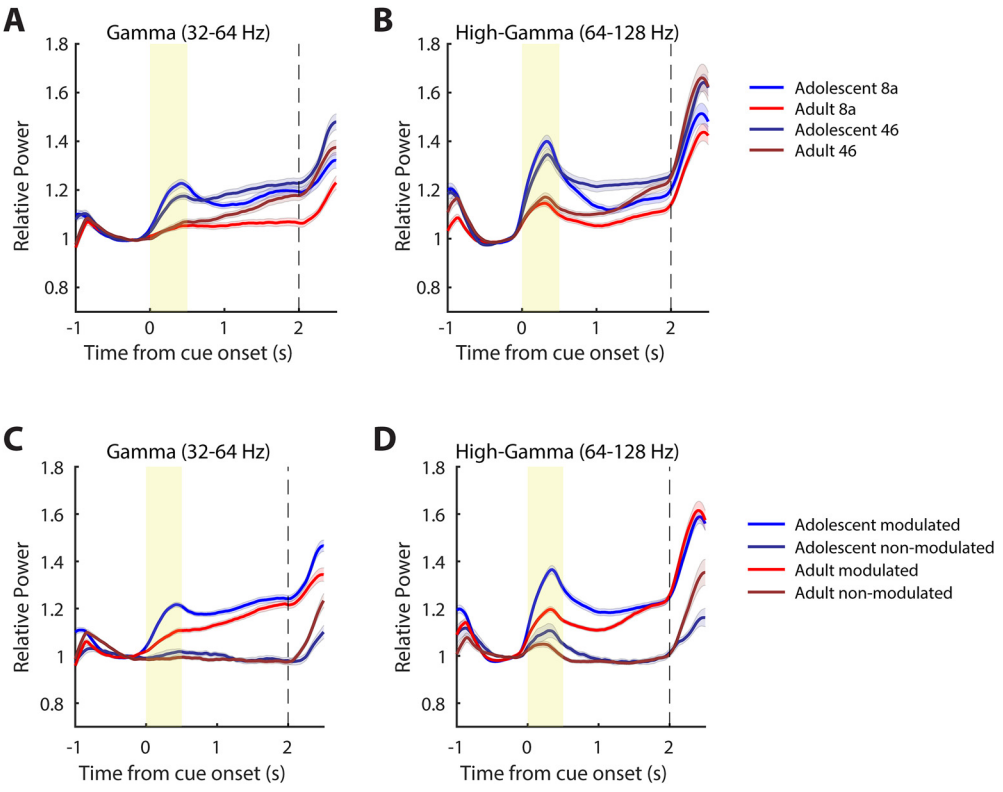

Figure 4. LFP power changes across different anatomic regions and recording sites. ***A***, ***B***, LFP band power for all subjects recorded from area 8a ($N = 48$ adolescent sites; $N = 85$ adult sites) and area 46 ($N = 70$ adolescent sites; $N = 78$ adult sites), respectively. ***C***, ***D***, LFP band-power evolutions of sites grouped according to the level of changes (significant/nonsignificant) in gamma power (adolescent, 104/26; adult, 97/67) or high-gamma power (adolescent. 117/13; adult, 122/42), respectively, during the working memory delay. Shaded areas represent the SEM.

sampling of recording sites with heterogeneous LFP power properties, we defined a site to be LFP power modulated if its delay period power in a certain frequency band differed significantly relative to baseline (evaluated with a paired t test, at the $\alpha = 0.05$ significance level). Most adolescent and adult sites were gamma power modulated, though adolescent gamma power-modulated sites were more frequent (adolescent, 104 of 130; adult, 97 of 164; Fisher's exact test, $p = 1.4E\text{-}4$). A similar percentage of sites were power modulated in the high-gamma band (adolescent, 117 of 130; adult, 122 of 164; Fisher's exact test, $p = 8.1E\text{-}4$). We repeated the comparison of gamma power between the young and adult stages, including in the analysis, exclusively the power-modulated sites. A higher power in the adolescent stage than in the adult stage was still present in the gamma-frequency band (Fig. 4*C*; two-tailed t test: $t_{(199)} = 3.07$, $p = 2.5E\text{-}3$) and the high gamma-frequency band (Fig. 4*D*; two-tailed t test: $t_{(237)} = 3.31$, $p = 1.1E\text{-}3$). The observed differences in gamma and high-gamma delay power were thus unlikely because of unequal sampling of modulated versus nonmodulated sites.

Differences between developmental stages did not only involve the mean spectral power; generally higher variance of gamma powered was observed in the young stage, particularly for the cue period (two-sample F test for equal variances $F_{(129,163)} = 1.65$, $p = 2.7E\text{-}3$); adult stage variance was also higher in the delay period, but it did not reach statistical significance ($F_{(129,163)} = 1.16$, $p = 0.36$).

Spectral power and behavior

Since the adult stage was characterized by a higher level of performance, it was of interest to determine how performance influenced the observed differences in LFP power. It has been previously reported that differences in neuronal firing rate between developmental stages were evident even when task performance differences were controlled for (Zhou et al., 2016c). Similarly, we matched the performance between sessions from the adolescent and adult stages by subsampling the top and bottom 37% of sessions from the two stages respectively. This resulted in two sets of sessions with highly comparable average performance (adolescent, 96.5%; adult, 96.5%). As shown in Figure 5, *A* and *B*, the time course of LFP power as well as its changes across developmental stages were similar in this subset and the whole population of recording sites. Specifically, a decrease of gamma-band power in the adult stage was evident even in this subset of sessions, equalized for performance. Subject KE had both the largest task performance improvement across stages as well as the strongest decrease in gamma- and high gamma-band power. However, when performance was matched between stages for individual subjects, the gamma power decrease in the adult stage was still present (Fig. 5*C*,*D*).

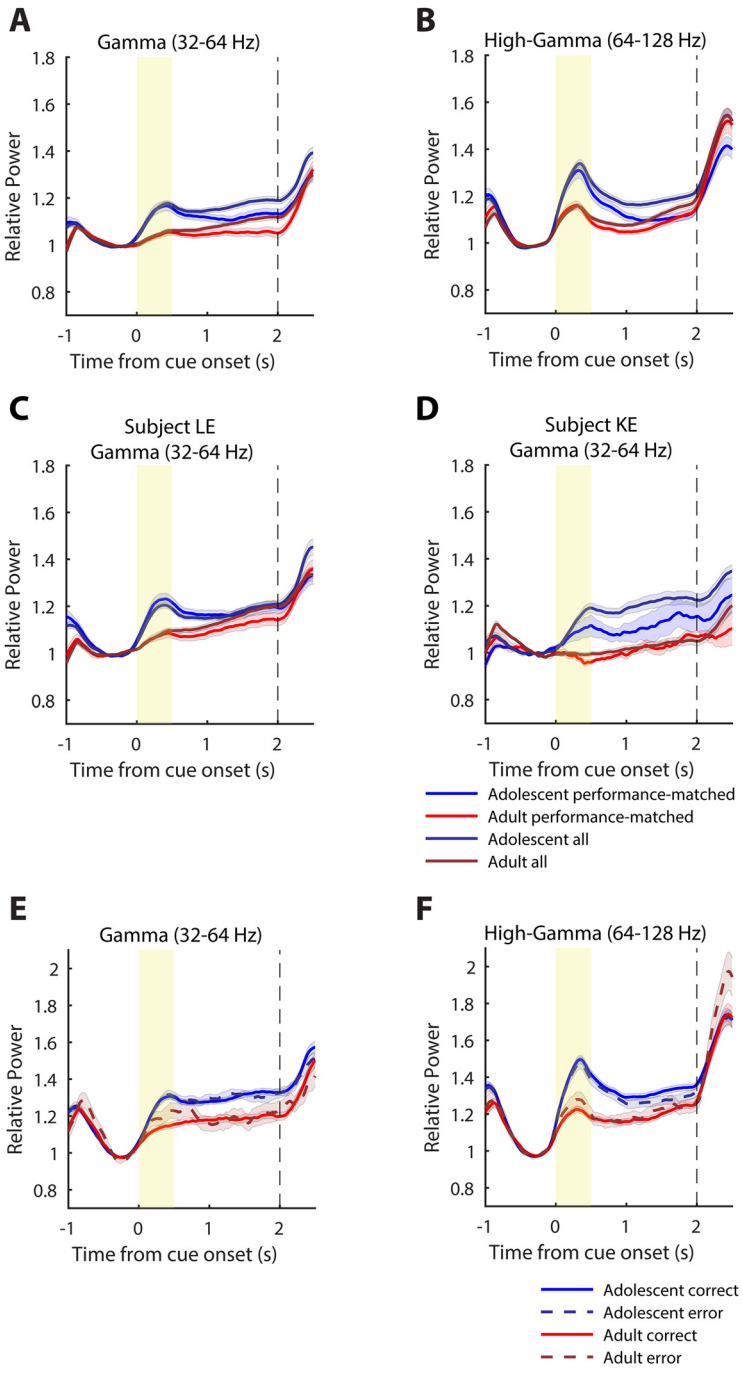

Figure 5. LFP power changes across developmental stages are not accounted for by performance. ***A***, ***B***, Average temporal evolution of LFP gamma- and high gamma-band power from a subset of sessions (37% of sessions from each developmental stage) where the average task performance was the same between the adolescent and the adult stages. ***C***, ***D***, Average LFP gamma-band power for subjects LE and KE, respectively, from a subset of sessions where the average task performance was the same between the adolescent and the adult stages. ***E***, ***F***, Average LFP gamma-band and high gamma-band power for correct and saccadic error trials, respectively. Only correct trials for the same cue location in the corresponding session as the error trials were included.

We similarly compared LFP power in correct and error trials. We identified sessions where recordings included sufficient error trials (excluding breaks in fixation, which resulted in aborted trials) from the adolescent ($N = 127$) and adult ($N = 90$) stages, respectively. For each session, average LFP power was computed

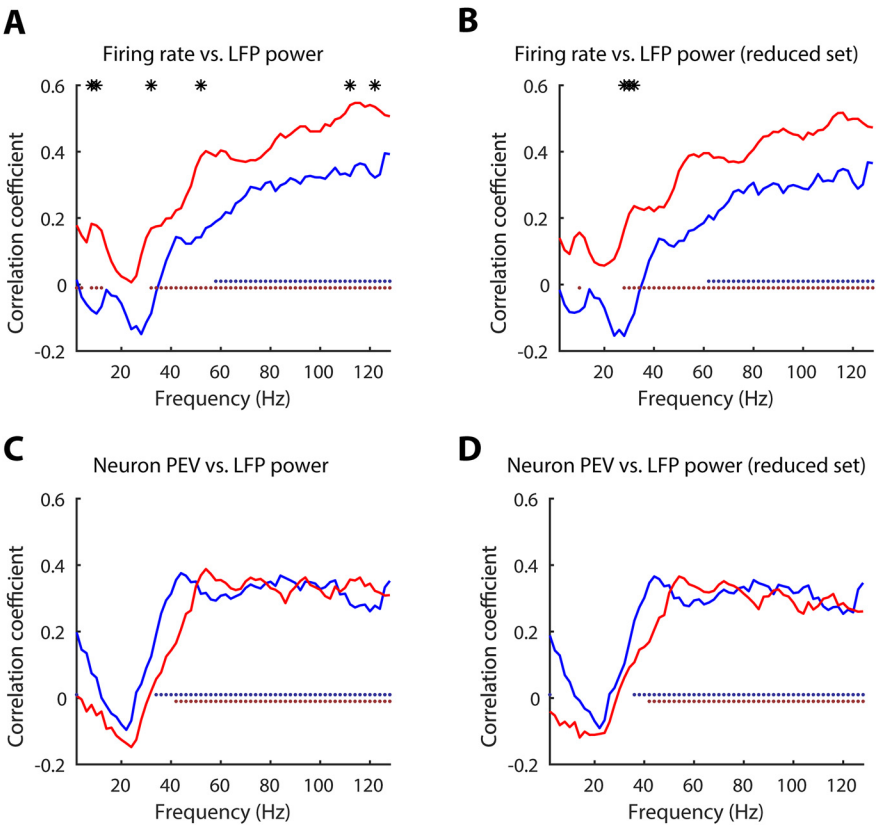

Figure 6. Neuron-by-neuron correlations between spiking activity and LFP power. ***A***, Spearman's correlation coefficient between neuronal firing rate and LFP power for signals recorded from the same electrode. ***C***, Spearman's correlation coefficient between neuronal PEV and LFP power for signals recorded from the same electrode. ***B***, ***D***, Same as ***A*** and ***C***, but for a firing rate-matched subset of neurons. Solid dots indicate significant correlations (Bonferroni–Holm-corrected type I error rate, <0.05). Asterisks stand for significant differences between the adolescent and the adult (Fisher's Z transform, Bonferroni–Holm-corrected type I error rate, < 0.05).

using the error trials and compared against that computed from the correct trials matched for stimulus location in that same session (Fig. 5*E*,*F*). The LFP power in all bands remained similar between the error and correct trials throughout the cue and delay epochs. As a result, the between-stage differences in gamma power were evident for both correct and error trials. These results indicated that task performance alone could not explain the differences seen in LFP band power.

Adolescent neuron delay period firing correlates less with gamma

Gamma oscillations have been suggested to reflect the underlying synchronization of local networks, giving rise to delay period activity as well as differential encoding of stimulus information in working memory (Roux and Uhlhaas, 2014). Given that higher firing rate was present in the delay period during the adult stage (Zhou et al., 2016c), it seemed curious that delay period gamma power and firing rate saw changes in opposite directions during adolescent development. Therefore, we tested for potential changes in correlation at the neuronal population level between gamma-power modulation and neuronal spiking. The preferred stimulus location of a neuron was defined as the one that evoked the highest average firing rate in the cue and delay periods combined. The correlation between neuronal firing and LFP power was overall higher in the adult and emerged among a broader band of frequencies (Fig. 6*A*). In the adult stage, the evoked delay period firing rates of neurons to the preferred stimulus location weakly but significantly correlated with gamma (Spearman's $\rho = 0.326$, $p =$ 4.0E-11) and high-gamma power modulations in LFP signals recorded at the corresponding sites (Spearman's $\rho = 0.513$, $p = 1.2$E-27). The strength of such correlations was weaker in the adolescent stage for the gamma (Spearman's $\rho =$ 0.170, $p =$ 0.003) and high-gamma (Spearman's $\rho =$ 0.360, $p = 1.6$E-10) bands, respectively. The adult correlation between delay period firing rate and high gamma-band LFP was significantly higher than the young one (Fisher's Z-transform: gamma, $p = 0.031 > 0.05/2$; high gamma, $p = 0.014 < 0.05/2$ under Bonferroni correction).

To discount the potential contribution of firing rate differences (adolescent, 5.79 ± 7.04 spikes/s; vs adult, 7.44 ± 8.28 spikes/s) to gamma power through spectral leakage, we assembled an evoked firing rate-matched subset of data by removing the top 5.6% of adult neurons (22 of 392) and the bottom 5.0% of adolescent neurons (15 of 298) in terms of evoked firing rate in the delay period to the preferred stimulus location. These remaining adolescent neurons had an average evoked firing rate of 6.16 ± 7.04 spikes/s, matching the 6.01 ± 5.49 spikes/s of the remaining adult neurons (two-tailed t test: $t_{(651)} = 0.32$, $p = 0.75$). The delay-evoked firing of the reduced dataset showed a very similar pattern of correlations (Fig. 6*B*) as the full dataset between gamma power modulations (adolescent: Spearman's $\rho = 0.160$, $p = 0.007$; adult: Spearman's $\rho = 0.335$, $p = 4.0$E-11) and high-gamma power modulations (adolescent: Spearman's $\rho = 0.339$, $p = 4.9$E-9; adult: Spearman's $\rho = 0.490$, $p = 1.0$E-23). After matching for evoked neuronal firing rates, the adult stage still showed significantly stronger correlations than the adolescent one (Fisher's Z-transform: gamma, $p = 0.\ 018 < 0.05/2$; high gamma, $p = 0.021 < 0.05/2$ under Bonferroni correction). Furthermore, these differences in correlation cannot be explained by the mismatch of the gamma power of two stages either, for the higher gamma-power average of the adolescents should lead to higher correlation coefficients if the underlying true distribution of correlations were the same between the two stages. This analysis demonstrates that, although the delay period activity reflected in gamma power was lower in the mature PFC, there was an increased activity alignment between individual neurons and the local network. This could suggest a more efficient information encoding scheme: in response to a given stimulus, neurons not encoding relevant information become suppressed, resulting in a less noisy, yet more efficient population code. We test this hypothesis in the next section by examining information encoding in PFC neural activity. The results of this analysis suggest that network activity may be constraining unit responses more in the adult stage than the adolescent stage.

Delay period neuronal information encoding is associated with greater gamma power

LFP power in the delay period is often tuned for the spatial location of the stimulus (Pesaran et al., 2002), and such tuning was

indeed found in our dataset, as well. Gamma and high-gamma power, in general, exhibited unimodal tuning curves (Fig. 7*A*,*B*) similar to those of neuronal firing (Fig. 7*C*). We therefore wished to test whether the higher adolescent gamma power was only evident in sites selective for the stimulus location or in sites that were not modulated by the stimulus. We defined spatially selective LFP sites as those in which delay period power differed significantly depending on the location of the stimulus (evaluated with one-way ANOVA at the $\alpha = 0.05$ significance level). Similar percentages of adolescent and adult LFP sites exhibited spatially selective gamma power (adolescent, 31 of 130 sites; adult, 28 of 164 sites) and high-gamma power (adolescent, 41 of 130 sites; adult, 52 of 164 sites). Among the spatially selective sites, the adolescent and adult gamma power had highly similar responses to their preferred cue locations (two-tailed *t* test: $t_{(57)} = 0.33$, $p = 0.74$). Across response to all cue locations, the average delay period gamma power was marginally higher in the adolescent and did not reach significance (two-tailed *t* test: $t_{(57)} = 0.78$, $p = 0.44$). This was because of the adult gamma power showed a slight decrease to nonpreferred cue locations, resulting in a slightly sharper delay period tuning. High-gamma power at the high-gamma power-selective sites also showed only modest power decrease in the adult at the preferred cue location (two-tailed *t* test: $t_{(57)} = 1.90$, $p = 0.06$). On the other hand, delay period LFP power changed more prominently among the non-spatially selective sites, being significantly higher in the adolescent stage for both the gamma (two-tailed *t* test: $t_{(233)} = 5.31$, $p = 2.6\text{E-}7$) and high-gamma frequency band (two-tailed *t* test: $t_{(199)} = 3.89$, $p = 1.4\text{E-}4$).

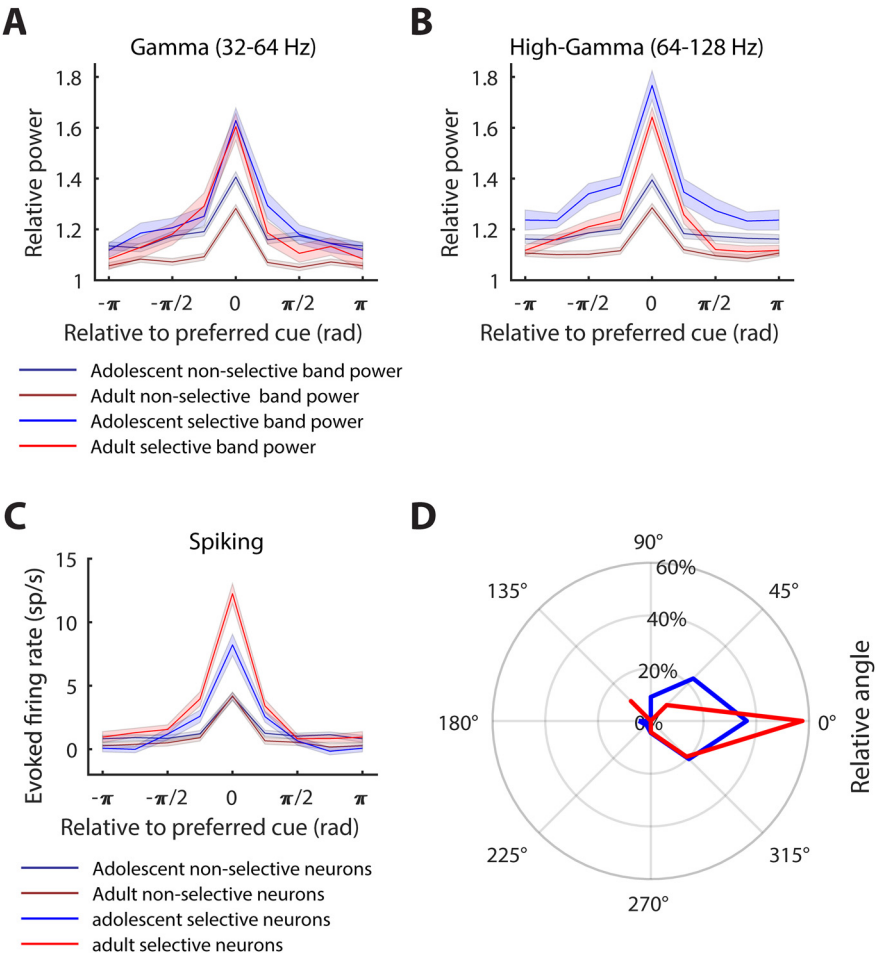

Figure 7. Developmental changes of delay period information encoding in LFP band power and neuronal spiking. ***A***, Tuning curves of delay period LFP gamma band power aligned to the preferred cue location of each recording site. Sites were grouped according to developmental stage as well as whether the delay period power was significantly tuned. ***B***, Same as ***A*** but for high-gamma power. ***C***, Tuning curves of evoked delay period firing rate aligned to the preferred cue location for each neuron. Neurons were grouped according to developmental stage as well as whether the delay period firing rate was significantly tuned. ***D***, The distribution of angle differences between the preferred cue location of gamma power and the evoked firing rate of neurons for the adolescent stage (blue) and adult stage (red) among the coexisting, spatially selective LFP sites and neurons.

In analogy to spatially selective LFP sites, we identified spatially selective single neurons if their average evoked firing rates in the delay period were significantly different across stimulus locations and "nonselective" otherwise (see Materials and Methods). This resulted in 39% of adolescent neurons (116 of 298) and 40% of adult neurons (157 of 392) being categorized as spatially selective. The ratio of selective to nonselective neurons did not differ significantly between the two stages (Fisher's exact test, $p = 0.81$). The firing rates of all neurons as well as selective neurons are shown in Figure 8*A*–*C*. Among the selective neurons, those in the adult stage had higher evoked firing rates in the delay period to their preferred stimulus locations (Fig. 8*B*; two-tailed *t* test: $t_{(271)} = 2.98$, $p = 0.003$) as well as higher PEV (Fig. 8*D*; two-tailed *t* test: $t_{(271)} = 2.71$, $p = 0.007$). We used a two-way ANOVA to compare delay period LFP power in sites where selective and nonselective neurons were recorded (Fig. 9*A*–*D*). LFP delay period gamma (Fig. 9*C*) and high-gamma (Fig. 9*D*) power levels were higher at sites where selective neurons were recorded, evidenced by a significant main effect of selective-neuron site (gamma: $F_{(1,290)} = 24.78$, $p = 1.1\text{E-}6$; high gamma: $F_{(1,290)} = 25.04$, $p = 9.8\text{E-}7$). There was also a significant main effect of developmental stage (gamma: $F_{(1,290)} = 24.85$, $p = 1.1\text{E-}6$; high gamma: $F_{(1,290)} = 22.42$, $p = 3.4\text{E-}6$), but no interaction between the selective neuron site and developmental stage (gamma: $F_{(1,290)} = 3.30$, $p = 0.07$; high gamma: $F_{(1,290)} = 0.16$, $p = 0.69$).

Such systemic effect could have been underlain by the preference of selective neurons for gamma modulation. Indeed, selective neurons were more likely to be found at gamma-modulated recording sites compared with nonselective neurons in both the adolescent stage (selective neurons: 95.7%, $N = 116$; nonselective neurons: 85.7%, $N = 182$; Fisher's exact test, $p = 0.006$) and the adult stage (selective neurons: 74.5%, $N = 157$; nonselective neurons: 58.3%, $N = 235$; Fisher's exact test, $p = 0.001$).

To further investigate the functional implications of such changes, we identified recording sites with coexisting, spatially selective gamma LFP power and neurons, and extracted the preferred stimulus location for each signal respectively. Interestingly, the preferred stimulus angles became more aligned (Fig. 7*D*; Fisher's exact test, $p = 0.059$) between gamma power and spiking in the adult (27 of 47) than the adolescent (16 of 44).

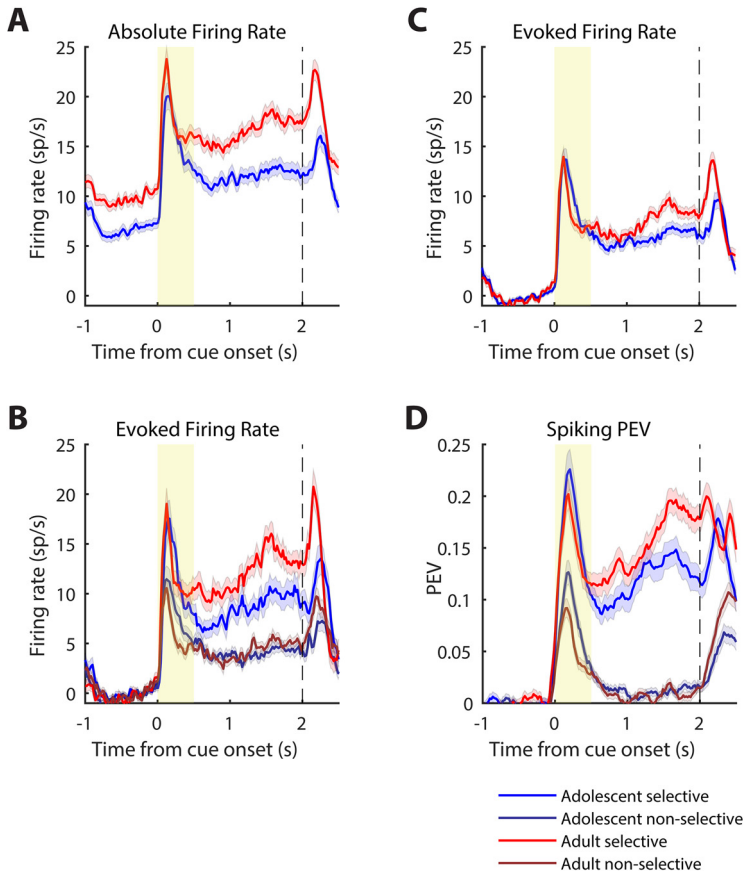

Figure 8. Neuronal spiking and information encoding in the ODR task. ***A***, ***C***, Population averages of neuronal raw firing rate and evoked firing rate by subtracting the average in the 1 s fixation period for neurons recorded in the adolescent ($N = 298$) and adult ($N = 392$) stages. ***B***, ***D***, Average evoked firing rate and PEV by cue location after dividing the neurons according to differential delay period firing (selective/nonselective) in the adolescent (116/182) and adult (157/235) stages.

A frequency-by-frequency examination of the correlation between LFP power and the PEV of neuronal discharges (Fig. 6*C*) revealed that for both the adolescent and adult neurons, there was significant correlation between neuronal information and LFP power in the gamma and high-gamma frequency range (Bonferroni–Holm-corrected type I error rate, <0.05). Similar to the findings above based on band-specific LFP power, no significant difference was found between the adolescent and the adult at any frequencies (Fisher's *Z* transform, Bonferroni–Holm corrected), indicating that the association between gamma power and neuronal information encoding remained highly similar in both developmental stages. For the reduced dataset with matched firing rates for the adolescent and adult neurons, the distribution of correlations was still highly consistent between the two stages (Fig. 6*D*). This result suggests that while the mature PFC represented the preferred stimulus information more efficiently, the fundamental relationship between the working memory delay period activity and LFP gamma power was present in both stages. To the same extent, increased gamma oscillations supported stronger information encoding in both the adolescent and adult stages.

No strong temporal correlation between LFP power modulations and neuronal spiking

LFP oscillations in the dlPFC have been previously suggested to control neuronal spiking and thus information encoding in a moment-by-moment fashion through their transient temporal dynamics (Lundqvist et al., 2016, 2018). To test, at the single-trial level, how much the delay period moment-by-moment change in gamma and high-gamma power reflected neuronal spiking, we extracted, for preferred stimulus trials of each neuron, their firing rate (convolved with a 50 ms boxcar kernel) and band power traces. On single trials, gamma power often exhibited short-living peaks surrounded by decreases in power. When single trials from all recording sites were pooled according to developmental stage, gamma power exhibited peak time points throughout the delay period (Fig. 10*A*,*B*). Both the adolescent and adult gamma power peak times followed a similar distribution (two-sample Kolmogorov–Smirnov test $D_{(6185)} = 0.03$, $p = 0.131$). The trial-by-trial spiking of the matching neurons on the other hand, showed no evidence of activity clustered at these gamma peaks and thus bore little temporal structure similarity (Fig. 10*C*,*D*). This was to be expected according to previous accounts of prefrontal neurons exhibiting higher temporal irregularity in the mnemonic delay period, the behavior of the majority of which mimics a Poisson process (Compte et al., 2003). Consequently, the delay period gamma power showed little to no correlation with neuronal firing at the corresponding recording sites in either the adolescent (Spearman's correlation, median $\rho = 0.04$; 25th and 75th percentiles = −0.11, 0.20; $N = 2792$) or adult stage (Spearman's correlation, median $\rho = 0.02$; 25th and 75th percentiles = −0.12, 0.18; $N = 3393$). Shuffling the trial pairings between the gamma power and firing rate for 100,000 iterations within in each age group (adolescent 95% confidence interval, −0.009 to 0.013; adult 95% confidence interval, −0.006 to 0.013) showed that the observed median correlations were significantly higher than chance.

Similar analysis was conducted on the temporal profile of high-gamma power (Fig. 10*E*–*H*). Interestingly, the distribution of peaking time differed significantly between the two stages (two-sample Kolmogorov–Smirnov test: $D_{(6185)} = 0.08$, $p = 1E\text{-}9$), with the adolescent high-gamma power peaking earlier overall in the mnemonic delay. Furthermore, there was a weak temporal correlation between high-gamma power and neuronal firing at both the adolescent stage (Spearman's correlation, median $\rho = 0.13$; 25th and 75th percentiles = −0.04, 0.29; $N = 2792$) and adult stage (Spearman's correlation, median $\rho = 0.11$; 25th and 75th percentiles = −0.05, 0.27; $N = 3393$). Such correlations were abolished once the trial pairings were shuffled 100,000 times for either the adolescent trials (95% confidence interval, −0.010 to 0.013) or adult trials (95% confidence interval, −0.002 to 0.017).

While the correlation between high-gamma power and firing rate is a common observation (Ray and Maunsell, 2011), the absolute level of correlation observed in this dataset was rather low. Furthermore, spectral leakage from spiking might be responsible for part of this correlation, which would further reduce the magnitude of any true correlations. A frequency-by-frequency inspection of temporal correlations between neuronal firing and LFP powers showed that the correlation coefficient increased with frequencies for both the adolescent and the adult, further suggesting the possible contribution of spectral leakage

from spikes at higher frequencies (Fig. 11). The positive correlations became significantly different from 0 starting at 36 and 42 Hz for the adolescent and the adult, respectively. It is also worth noting that, opposite to the developmental effect on neuron-by-neuron correlations, the temporal correlation between LFP power and spiking was higher for the adolescent than the adult, mostly in the high-gamma range. This is further evidence that the stronger association between gamma power and high-firing neurons in the adult was not because of spectral leakage into the LFP directly from spiking activity. In summary, gamma power and neuronal spiking did not follow closely the same temporal profile from trial to trial. The relationship between the temporal dynamics of neuronal stimulus encoding and moment-by-moment LFP power modulation in the delay period showed a wide distribution and were not governed by a single rule across neurons. The adolescent and adult stages only seemed to differ in the distribution of the peak timing of high-gamma power from trial to trial.

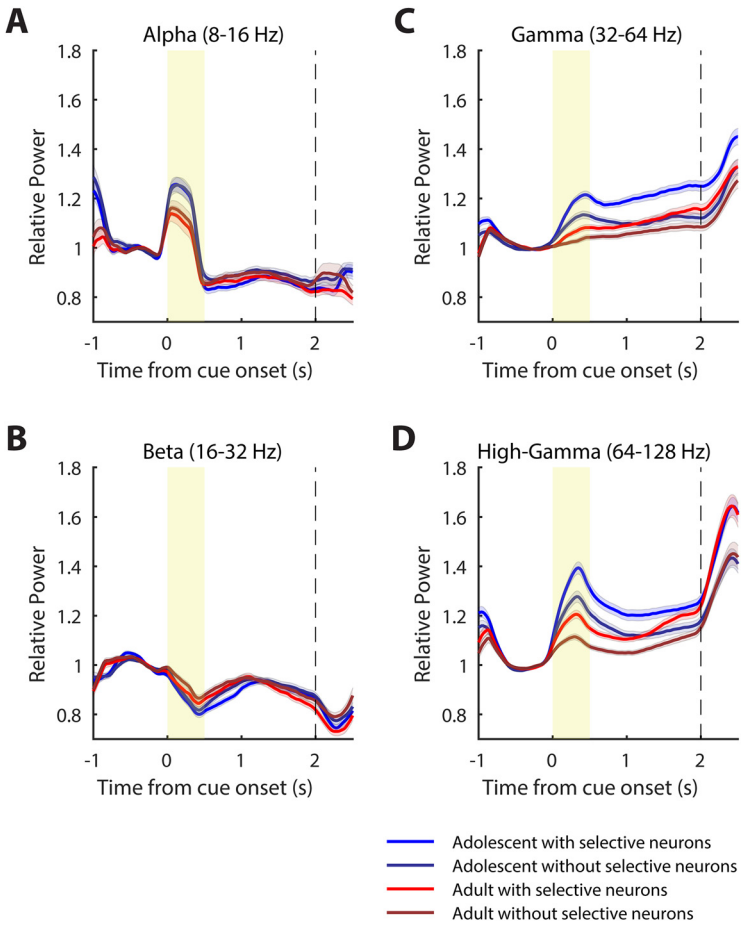

Figure 9. LPF power modulation as a function of neuronal information encoding. ***A–D***, Time course of LFP power in the alpha, beta, gamma, and high-gamma bands, respectively, of sites grouped according to whether spatially selective neurons were recorded at the corresponding sites (selective/nonselective) in the adolescent (69/61) and adult (77/87) stages.

Discussion

Working memory ability improves between adolescence and adulthood, a change generally attributed to maturation of the prefrontal cortex (Jaffe and Constantinidis, 2021). Previous studies have documented that the adult dlPFC is characterized by an increased delay period firing rate (Zhou et al., 2016c). We now saw an overall decrease of LFP gamma-band power in the delay period of the task in adult monkeys. A similar change was present for high-gamma power, while alpha- and beta-band power remained relatively stable. This gamma-power decrease was present both in more posterior prefrontal sites, in area 8a, as well as in more anterior ones, in area 46, which generally rank higher in the cortical hierarchy (Riley et al., 2017). The effect was not specifically tied to performance, suggesting that the mature PFC consistently generates lower-power gamma oscillations, even in sessions equalized for performance, and in error trials as well as correct. However, it should be noted that at the adult stage, the subjects had been exposed to more cumulative experience with the task.

The decrease in gamma power was specific for those sites not active during the encoding of information in working memory in the mature PFC. In both the adolescent and adult dlPFC, gamma power was higher at sites where neuronal spiking contained significant stimulus information in the delay period. These findings, combined with the observation that the two stages had almost identical percentages of selective neurons, indicate that stronger gamma oscillations would emerge in a local network of neurons actively maintaining task-relevant stimulus information throughout development. Rather, the adult PFC differed from the adolescent by having high-firing, information-encoding neurons more heavily distributed at sites with stronger gamma power. Among those sites and neurons with spatial selectivity, the encoded cue location was also more consistent between the single-unit firing and the LFP gamma power. Furthermore, the mature delay period firing rate increase was biased for selective neurons. This functional maturation at both the unit and network levels could work in synergy to support a potential refinement strategy in adulthood: compared with the immature dlPFC, the adult prefrontal cortex can more efficiently recruit a task-relevant subset of local networks, while reducing the activity of irrelevant populations. As a result, reverberatory dynamics are more localized and less diffuse, hence the lower magnitude of gamma power in population measures such as the LFP. These universal differences seen across all recording sites are likely to be underlain by overall changes in synaptic properties including synaptogenesis and receptor expression (Lewis et al., 2004; Hoftman and Lewis, 2011; Gonzalez-Burgos et al., 2015), leading to a shift in the excitation–inhibition balance and, consequently, in the level of neural synchronization (Compte et al., 2000).

Origins of LFP gamma power

The temporal relationship between neuronal spiking and gamma power is complex. During stimulus presentation, the highly correlated bottom-up inputs can serve to synchronize population neuronal spiking and phases of synchronized excitation by pyramidal neurons followed by inhibition by interneurons can thus produce oscillations in the field potentials (Fries, 2009). However, LFP gamma power can also emerge in the delay period, when no sensory input is present, and the postsynaptic potentials are dominated by the local recurrent connections

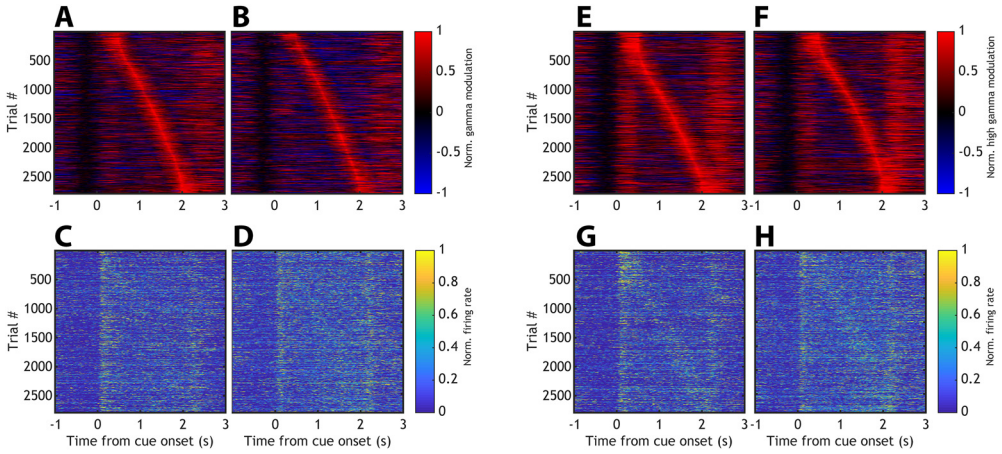

Figure 10. Trial-by-trial temporal evolution of neuronal firing and matched LFP power. ***A***, Adolescent single-trial gamma-band power arranged according to peak timing in the delay period ($N = 2792$). ***B***, Same as ***A*** for the adult LFP ($N = 3393$). ***C***, ***D***, Normalized neuronal firing rate (convolved with a 50 ms boxcar kernel) corresponding to the same trials in ***A*** and ***B***. ***E–H***, Same as ***A–D*** for high-gamma power.

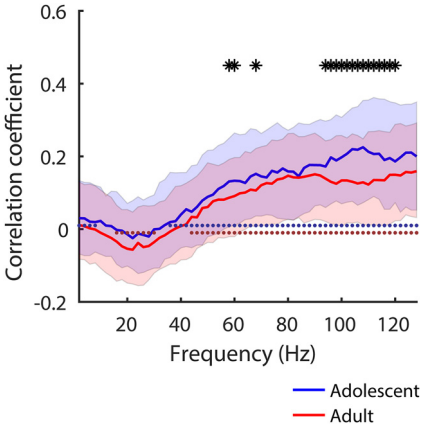

Figure 11. Average temporal correlation of LFP power with neuronal spiking. Solid lines are median Spearman's correlation coefficients for the adolescent and adult stages, respectively. Shaded areas are between the 25th and 75th percentiles. Solid dots indicate median correlations significantly different from zero (signed-rank test, Bonferroni–Holm-corrected type I error rate, <0.05). Asterisks stand for significant differences between the adolescent and the adult (Wilcoxon rank-sum test, Bonferroni–Holm-corrected type I error rate, <0.05).

(Pesaran et al., 2002). As modeling findings have suggested, high-frequency oscillations readily emerge in a strongly recurrent network in which single-neuron firing is highly irregular, without exhibiting synchronization among a sparsely sampled subset of neurons (Wang, 2010). Previous recordings have described Poisson-like dlPFC firing during the delay (Compte et al., 2003) and Fano factor values >1 for the adolescent and adult neurons alike (Zhou et al., 2016c). The spatial scope of LFP signals dictates that they reflect the summation of activity from a wide range of neurons (Kajikawa and Schroeder, 2011). Given the highly irregular nature of dlPFC neuronal firing, it is reasonable that LFPs would not be highly predictive of activity recorded from a small subset of single neurons from the local population of unsynchronized firing and various stimulus tuning. This was also supported by the fact that a smaller percentage of LFP sites showed significant spatial tuning compared with that of neuronal spiking.

Local-circuit differences have been described between adolescent and adult monkeys that could explain changes in persistent discharges and gamma-band LFP oscillations between developmental stages (Li et al., 2020). Zero-lag spiking synchronization based on cross-correlation analysis of nearby neurons (recorded at distances between 0.5 and 1 mm from each other) is markedly lower in adolescent monkeys than in adult monkeys. This difference is primarily the effect of changes in inhibitory interactions, the net efficacy of which declines in adulthood (Zhou et al., 2014). Anatomical evidence, in turn, implicates decreases in the connectivity strength of pyramidal neurons onto interneurons, which lessens the net output of inhibitory connections as the prefrontal cortex matures (Gonzalez-Burgos et al., 2015). This pruning of synaptic interactions implies less synaptic drive overall, which could explain our current finding of decreased rather than increased gamma-band power in the LFP.

Cognitive processes related to gamma power maturation

Results from human EEG/MEG literature have indicated systematic changes in rhythmicity between developmental stages, generally suggestive of higher gamma power in adulthood. However, closer examination of these studies reveals that the existence and direction of change in gamma power is not universal, but is dependent on the specific brain region, task epoch, and nature of the task performed. Many developmental EEG studies used resting-state EEG that reflects the network at a different state compared with when it is actively engaged in a working memory task or relied on passive sensory tasks, which revealed the greatest effects in lower cortical areas, including stronger adult 40 Hz auditory steady-state response dominantly generated in the auditory cortex and visually evoked gamma (30–148 Hz) oscillation amplitude in the occipital lobe (Uhlhaas and Singer, 2011). Task-dependent changes involving higher-order cognitive functions often saw effects that were differentiable between frontal and parietal regions (Roux and Uhlhaas, 2014). The working memory load-dependent gamma power (50–100 Hz) change reported by Kornblith et al. (2016) differed between task epochs and brain regions. During and immediately after cue presentation, gamma power increased with higher memory load in the parietal cortex but decreased with higher memory load in the prefrontal cortex, while in the late delay period, there was no significant load-dependent gamma power changes in either brain area. Uhlhaas et al. (2009) reported age-dependent gamma (30–75 Hz) power changes in a face perception task for parietal electrodes only. Furthermore, the task effect can be feature specific. Honkanen et al. (2015) saw load-dependent increases of gamma (40–72 and 80–120 Hz) power for color and shape features but a decrease for

location features. At least some preliminary evidence exists for decreases in EEG gamma power in the delay period of the oculomotor delayed response task across human adolescent development (McKeon et al., 2020).

Oscillatory discharges increase early in postnatal development in nonhuman primates, as inferred by intracellular recording experiments in slice preparations (Gonzalez-Burgos et al., 2015). It is possible therefore that gamma oscillations follow an inverted U curve during development. Gamma power has also been described in other animal models e.g., revealing a monotonic postnatal increase in prefrontal gamma power in some rodent studies (Bitzenhofer et al., 2020). However, key differences have been discovered between animal models in the developmental profile of excitatory–inhibitory circuits, including the lack of NMDA receptors on adult frontal interneurons (Wang and Gao, 2009) as well as GABA synaptogenesis and functional maturation being complete well before the onset of adolescence in the rodents (Le Magueresse and Monyer, 2013).

Abnormally lower gamma power is commonly observed in schizophrenia (Woo et al., 2010; Uhlhaas and Singer, 2013), generally attributed to a shift of the excitation–inhibition balance toward a more excitable cortical state (Lisman, 2012). The decrease in gamma power is specific for stimulus presentation and task engagement in patients with schizophrenia (Uhlhaas and Singer, 2010); spontaneous gamma power may be elevated in these patients, as it is during psychotic episodes and auditory hallucinations (Baldeweg et al., 1998; Spencer et al., 2009; Grent-'t-Jong et al., 2018). In this context, our results would suggest that the primate adolescence represents a state in the opposite end of the excitation/inhibition spectrum, dominated by greater inhibition, which is again consistent with the idea of elevated inhibitory drive in adolescence (Zhou et al., 2014). In turn, this result would suggest that schizophrenia represents an aberrant, excessive decrease in inhibition, rather than a prolonged adolescent-like state that failed to mature.

These results suggest that during brain maturation, there might be systematic changes at the molecular and/or network level prominent enough to mask changes in features specific to a cognitive function of the brain region of interest. These effects would be especially challenging to differentiate when only macroscopic measures of neural activity are adopted. Bridging the processes underlying rhythmicity from the neuron to the circuit level will be an important goal of future studies.

References

Anderson SA, Classey JD, Condé F, Lund JS, Lewis DA (1995) Synchronous development of pyramidal neuron dendritic spines and parvalbumin-immunoreactive chandelier neuron axon terminals in layer III of monkey prefrontal cortex. Neuroscience 67:7–22.

Baldeweg T, Spence S, Hirsch SR, Gruzelier J (1998) Gamma-band electroencephalographic oscillations in a patient with somatic hallucinations. Lancet 352:620–621.

Bitzenhofer SH, Pöpplau JA, Hanganu-Opatz I (2020) Gamma activity accelerates during prefrontal development. Elife 9:e56795.

Bourgeois JP, Goldman-Rakic PS, Rakic P (1994) Synaptogenesis in the prefrontal cortex of rhesus monkeys. Cereb Cortex 4:78–96.

Bunge SA, Dudukovic NM, Thomason ME, Vaidya CJ, Gabrieli JD (2002) Immature frontal lobe contributions to cognitive control in children: evidence from fMRI. Neuron 33:301–311.

Burgund ED, Lugar HM, Miezin FM, Schlaggar BL, Petersen SE (2006) The development of sustained and transient neural activity. Neuroimage 29:812–821.

Buzsáki G, Wang XJ (2012) Mechanisms of gamma oscillations. Annu Rev Neurosci 35:203–225.

Compte A, Brunel N, Goldman-Rakic PS, Wang XJ (2000) Synaptic mechanisms and network dynamics underlying spatial working memory in a cortical network model. Cereb Cortex 10:910–923.

Compte A, Constantinidis C, Tegnér J, Raghavachari S, Chafee MV, Goldman-Rakic PS, Wang XJ (2003) Temporally irregular mnemonic persistent activity in prefrontal neurons of monkeys during a delayed response task. J Neurophysiol 90:3441–3454.

Constantinidis C, Luna B (2019) Neural substrates of inhibitory control maturation in adolescence. Trends Neurosci 42:604–616.

Davidson MC, Amso D, Anderson LC, Diamond A (2006) Development of cognitive control and executive functions from 4 to 13 years: evidence from manipulations of memory, inhibition, and task switching. Neuropsychologia 44:2037–2078.

Dienel SJ, Lewis DA (2019) Alterations in cortical interneurons and cognitive function in schizophrenia. Neurobiol Dis 131:104208.

Fries P (2009) Neuronal gamma-band synchronization as a fundamental process in cortical computation. Annu Rev Neurosci 32:209–224.

Fry AF, Hale S (2000) Relationships among processing speed, working memory, and fluid intelligence in children. Biol Psychol 54:1–34.

Gathercole SE, Pickering SJ, Ambridge B, Wearing H (2004) The structure of working memory from 4 to 15 years of age. Dev Psychol 40:177–190.

Giedd JN, Rapoport JL (2010) Structural MRI of pediatric brain development: what have we learned and where are we going? Neuron 67:728–734.

Goldman-Rakic PS (1994) Working memory dysfunction in schizophrenia. J Neuropsychiatry Clin Neurosci 6:348–357.

Gonzalez-Burgos G, Miyamae T, Pafundo DE, Yoshino H, Rotaru DC, Hoftman G, Datta D, Zhang Y, Hammond M, Sampson AR, Fish KN, Ermentrout GB, Lewis DA (2015) Functional maturation of GABA synapses during postnatal development of the monkey dorsolateral prefrontal cortex. Cereb Cortex 25:4076–4093.

Grent-'t-Jong T, Gross J, Goense J, Wibral M, Gajwani R, Gumley AI, Lawrie SM, Schwannauer M, Schultze-Lutter F, Navarro Schröder T, Koethe D, Leweke FM, Singer W, Uhlhaas PJ (2018) Resting-state gamma-band power alterations in schizophrenia reveal E/I-balance abnormalities across illness-stages. Elife 7:e37799.

Hoftman GD, Lewis DA (2011) Postnatal developmental trajectories of neural circuits in the primate prefrontal cortex: identifying sensitive periods for vulnerability to schizophrenia. Schizophr Bull 37:493–503.

Honkanen R, Rouhinen S, Wang SH, Palva JM, Palva S (2015) Gamma oscillations underlie the maintenance of feature-specific information and the contents of visual working memory. Cereb Cortex 25:3788–3801.

Howard MW, Rizzuto DS, Caplan JB, Madsen JR, Lisman J, Aschenbrenner-Scheibe R, Schulze-Bonhage A, Kahana MJ (2003) Gamma oscillations correlate with working memory load in humans. Cereb Cortex 13:1369–1374.

Huttenlocher PR, Dabholkar AS (1997) Regional differences in synaptogenesis in human cerebral cortex. J Comp Neurol 387:167–178.

Jaffe RJ, Constantinidis C (2021) Working memory: from neural activity to the sentient mind. Compr Physiol 11:2547–2587.

Jensen O, Kaiser J, Lachaux JP (2007) Human gamma-frequency oscillations associated with attention and memory. Trends Neurosci 30:317–324.

Kajikawa Y, Schroeder CE (2011) How local is the local field potential? Neuron 72:847–858.

Klingberg T, Forssberg H, Westerberg H (2002) Training of working memory in children with ADHD. J Clin Exp Neuropsychol 24:781–791.

Kornblith S, Buschman TJ, Miller E (2016) Stimulus load and oscillatory activity in higher cortex. Cereb Cortex 26:3772–3784.

Kwon H, Reiss AL, Menon V (2002) Neural basis of protracted developmental changes in visuo-spatial working memory. Proc Natl Acad Sci U S A 99:13336–13341.

Le Magueresse C, Monyer H (2013) GABAergic interneurons shape the functional maturation of the cortex. Neuron 77:388–405.

Lewis DA, Cruz D, Eggan S, Erickson S (2004) Postnatal development of prefrontal inhibitory circuits and the pathophysiology of cognitive dysfunction in schizophrenia. Ann N Y Acad Sci 1021:64–76.

Li S, Zhou X, Constantinidis C, Qi XL (2020) Plasticity of persistent activity and its constraints. Front Neural Circuits 14:15.

Lisman J (2012) Excitation, inhibition, local oscillations, or large-scale loops: what causes the symptoms of schizophrenia? Curr Opin Neurobiol 22:537–544.

Luna B, Thulborn KR, Munoz DP, Merriam EP, Garver KE, Minshew NJ, Keshavan MS, Genovese CR, Eddy WF, Sweeney JA (2001) Maturation of widely distributed brain function subserves cognitive development. Neuroimage 13:786–793.

Lundqvist M, Herman P, Warden MR, Brincat SL, Miller EK (2018) Gamma and beta bursts during working memory readout suggest roles in its volitional control. Nat Commun 9:394.

Lundqvist M, Rose J, Herman P, Brincat SL, Buschman TJ, Miller EK (2016) Gamma and beta bursts underlie working memory. Neuron 90:152–164.

McKeon S, Calabro F, Luna B (2020) Development of EEG-derived spectral processing of working memory through adolescence. In: 8th Annual Flux Virtual Congress Abstract Book, p 82. Victoria, BC, Canada: Podium Conference Specialists.

Olesen PJ, Macoveanu J, Tegnér J, Klingberg T (2007) Brain activity related to working memory and distraction in children and adults. Cereb Cortex 17:1047–1054.

Olesen PJ, Nagy Z, Westerberg H, Klingberg T (2003) Combined analysis of DTI and fMRI data reveals a joint maturation of white and grey matter in a fronto-parietal network. Brain Res Cogn Brain Res 18:48–57.

Pesaran B, Pezaris JS, Sahani M, Mitra PP, Andersen RA (2002) Temporal structure in neuronal activity during working memory in macaque parietal cortex. Nat Neurosci 5:805–811.

Ray S, Maunsell JH (2011) Different origins of gamma rhythm and high-gamma activity in macaque visual cortex. PLoS Biol 9:e1000610.

Riley MR, Qi XL, Constantinidis C (2017) Functional specialization of areas along the anterior-posterior axis of the primate prefrontal cortex. Cereb Cortex 27:3683–3697.

Roux F, Uhlhaas PJ (2014) Working memory and neural oscillations: α-γ versus θ-γ codes for distinct WM information? Trends Cogn Sci 18:16–25.

Spencer KM, Niznikiewicz MA, Nestor PG, Shenton ME, McCarley RW (2009) Left auditory cortex gamma synchronization and auditory hallucination symptoms in schizophrenia. BMC Neurosci 10:85.

Uhlhaas PJ, Roux F, Rodriguez E, Rotarska-Jagiela A, Singer W (2010) Neural synchrony and the development of cortical networks. Trends Cogn Sci 14:72–80.

Uhlhaas PJ, Roux F, Singer W, Haenschel C, Sireteanu R, Rodriguez E (2009) The development of neural synchrony reflects late maturation and restructuring of functional networks in humans. Proc Natl Acad Sci U S A 106:9866–9871.

Uhlhaas PJ, Singer W (2010) Abnormal neural oscillations and synchrony in schizophrenia. Nat Rev Neurosci 11:100–113.

Uhlhaas PJ, Singer W (2011) The development of neural synchrony and large-scale cortical networks during adolescence: relevance for the pathophysiology of schizophrenia and neurodevelopmental hypothesis. Schizophr Bull 37:514–523.

Uhlhaas PJ, Singer W (2013) High-frequency oscillations and the neurobiology of schizophrenia. Dialogues Clin Neurosci 15:301–313.

Ullman H, Almeida R, Klingberg T (2014) Structural maturation and brain activity predict future working memory capacity during childhood development. J Neurosci 34:1592–1598.

Wang X-J (2010) Neurophysiological and computational principles of cortical rhythms in cognition. Physiol Rev 90:1195–1268.

Wang H-X, Gao W-J (2009) Cell type-specific development of NMDA receptors in the interneurons of rat prefrontal cortex. Neuropsychopharmacology 34:2028–2040.

Woo T-UW, Spencer K, McCarley RW (2010) Gamma oscillation deficits and the onset and early progression of schizophrenia. Harv Rev Psychiatry 18:173–189.

Zhou X, Zhu D, Qi XL, Lees CJ, Bennett AJ, Salinas E, Stanford TR, Constantinidis C (2013) Working memory performance and neural activity in the prefrontal cortex of peri-pubertal monkeys. J Neurophysiol 110:2648–2660.

Zhou X, Zhu D, Katsuki F, Qi XL, Lees CJ, Bennett AJ, Salinas E, Stanford TR, Constantinidis C (2014) Age-dependent changes in prefrontal intrinsic connectivity. Proc Natl Acad Sci U S A 111:3853–3858.

Zhou X, Qi XL, Constantinidis C (2016a) Distinct roles of the prefrontal and posterior parietal cortices in response inhibition. Cell Rep 14:2765–2773.

Zhou X, Zhu D, King SG, Lees CJ, Bennett AJ, Salinas E, Stanford TR, Constantinidis C (2016b) Behavioral response inhibition and maturation of goal representation in prefrontal cortex after puberty. Proc Natl Acad Sci U S A 113:3353–3358.

Zhou X, Zhu D, Qi XL, Li S, King SG, Salinas E, Stanford TR, Constantinidis C (2016c) Neural correlates of working memory development in adolescent primates. Nat Commun 7:13423.